

1   **Evaporation, infiltration and storage of soil water in**  
2   **different vegetation zones in the Qilian Mountains: A**  
3   **stable isotope perspective**

4   **Guofeng Zhu<sup>1,2</sup>, Leilei Yong<sup>1,2</sup>, Xi Zhao<sup>1,2</sup>, Yuwei Liu<sup>1,2</sup>, Zhanxia Zhang<sup>1,2</sup>, Yuanxiao Xu<sup>1,2</sup>, Zhigang Sun<sup>1,2</sup>, Liyuan Sang<sup>1,2</sup>, Lei Wang<sup>1,2</sup>**

6   <sup>1</sup> College of Geography and Environment Science, Northwest Normal University, Lanzhou  
7   730070, China

8   <sup>2</sup> Shiyang River Ecological Environment Observation Station, Northwest Normal University,  
9   Lanzhou 730070, Gansu, China

10   **Correspondence to:** Guofeng Zhu (zhugf@nwnu.edu.cn)

11   **Abstract:** The processes of water storage have not been fully understood in different  
12   vegetation zones in mountainous areas, which is the main obstacle to further  
13   understanding hydrological processes and improving water resource assessments. To  
14   further understand the process of soil water movement in different vegetation zones  
15   (alpine meadow, coniferous forest, mountain grassland, and deciduous forest) in  
16   mountainous areas, this study monitored the temporal and spatial dynamics of  
17   hydrogen and oxygen stable isotopes in the precipitation and soil water of the Xiying  
18   River Basin. The results show that the order of soil water evaporation intensities in  
19   the four vegetation zones was mountain grassland ( $SWL_{slop}$ : 3.4) > deciduous forest  
20   ( $SWL_{slop}$ : 4.1) > coniferous forest ( $SWL_{slop}$ : 4.7) > alpine meadow ( $SWL_{slop}$ : 6.4). The  
21   soil water in the alpine meadow and coniferous forest evaporated from only the  
22   topsoil, and the rainfall input was fully mixed with each layer of soil. The evaporation  
23   signals of the mountain grassland and deciduous forest could penetrate deep into the  
24   middle, and lower layers of the soil as precipitation quickly flowed into the deep soil  
25   through the soil matrix. Each vegetation zone's water storage capacity of the 0-40 cm  
26   soil layer followed the order of alpine meadow (46.9 mm) > deciduous forest (33.0  
27   mm) > coniferous forest (32.1 mm) > mountain grassland (20.3 mm). In addition, the  
28   0-10cm soil layer has the smallest soil water storage capacity (alpine meadow:43.0  
29   mm; coniferous forest: 28.0 mm; mountain grassland: 17.5 mm; deciduous forest:

29.1 mm). This work will provide a new reference for understanding soil hydrology in  
arid headwater areas.

**Key words:** Xiying River; Stable isotope; Drought, Soil water storage

## 1. Introduction

In arid inland river basins, climate and vegetation changes will affect the hydrological cycle (Sharma et al., 2021; Tetzlaff et al., 2013). As an essential part of the water cycle, soil water in the unsaturated zone can be converted from precipitation into the stream or groundwater recharge. Determining soil water's evaporation, infiltration, and storage properties are critical to understand the regional hydrological cycle and water balance under climate and vegetation changes (Brooks et al., 2010; Dubbert and Werner, 2019; Grant and Dietrich, 2017).

As "fingerprints" of water, isotopes have been used to track ecohydrological characteristics, such as evaporation (Barnes and Allison, 1988; Zhu et al., 2021b), groundwater recharge (Koeniger et al., 2016), infiltration paths (Duvert et al., 2016; Tang and Feng, 2001; Zhu et al., 2021a), evapotranspiration distribution (Gibson et al., 2021; Xiao et al., 2018), and the water absorption by plants (Rothfuss and Javaux, 2017).

Water seepage in the unsaturated soil zone and water evaporation at the air–soil interface are the primary forms of soil water transport. The dynamic water process reflected by the displacement of the isotope signal on the soil profile is called the "memory effect". Understanding the "memory effect" will help us to trace the dynamic changes in climate and soil hydrology (Kleine et al., 2020). The change of stable isotopes in near-surface soil water may reflect the precipitation variation, but these variations decrease with depth unless there is preferential flow (Peralta-Tapia et al., 2015; Sprenger et al., 2016; Sprenger et al., 2017). Evaporation mainly occurred in the near-surface part of the soils (0–10 cm), and the light isotope molecules ( $^1\text{H}$  and  $^{16}\text{O}$ ) evaporated preferentially, resulting in the enrichment of heavy isotopes ( $^2\text{H}$  and  $^{18}\text{O}$ ) on the soil surface (Ferretti et al., 2003). Dansgaard (1964) proposed the concept of d-excess ( $\text{d-excess} = \delta^2\text{H} - 8\delta^{18}\text{O}$ ) to illustrate the intensity of evaporation

fractionation. Assuming that evaporation occurs in the atmosphere with a humidity of 75%, it shows that the d-excess value of atmospheric moisture accounts for the d-excess value of 10‰ in the atmospheric moisture, which conforms to the worldwide average isotopic labelling of meteoric waters. Landwehr and Coplen (2006) defined line conditioned excess as the difference between the  $\delta^2\text{H}$  value of the water sample and the  $\delta^{18}\text{O}$  linear transform value of the same sample, where the linear transformation reflects the relevant referenced meteoric water relationship. Compared with d-excess, lc-excess can explain the evaporative fractionation process better. The main reason is that lc-excess of precipitation and soil water changes smoothly and has relatively small seasonal changes (Landwehr et al., 2014). The dynamic changes of isotopes record the signal of soil water evaporation. This enrichment of this dynamic fractionation exists in soil water isotopes in different climatic regions. Compared with temperate regions, the evaporation signals in arid and Mediterranean environments penetrate deeper into the soil (Sprenger et al., 2016). After evaporation and seepage, some water is stored in the soil. The water storage capacity in humid areas is higher than that in arid areas, that in forest is higher than that in grassland, and that in surface soil layer is lower than that in deep soil layers with high clay content (Kleine et al., 2020; Milly, 1994; Snelgrove et al., 2021; Sprenger et al., 2019).

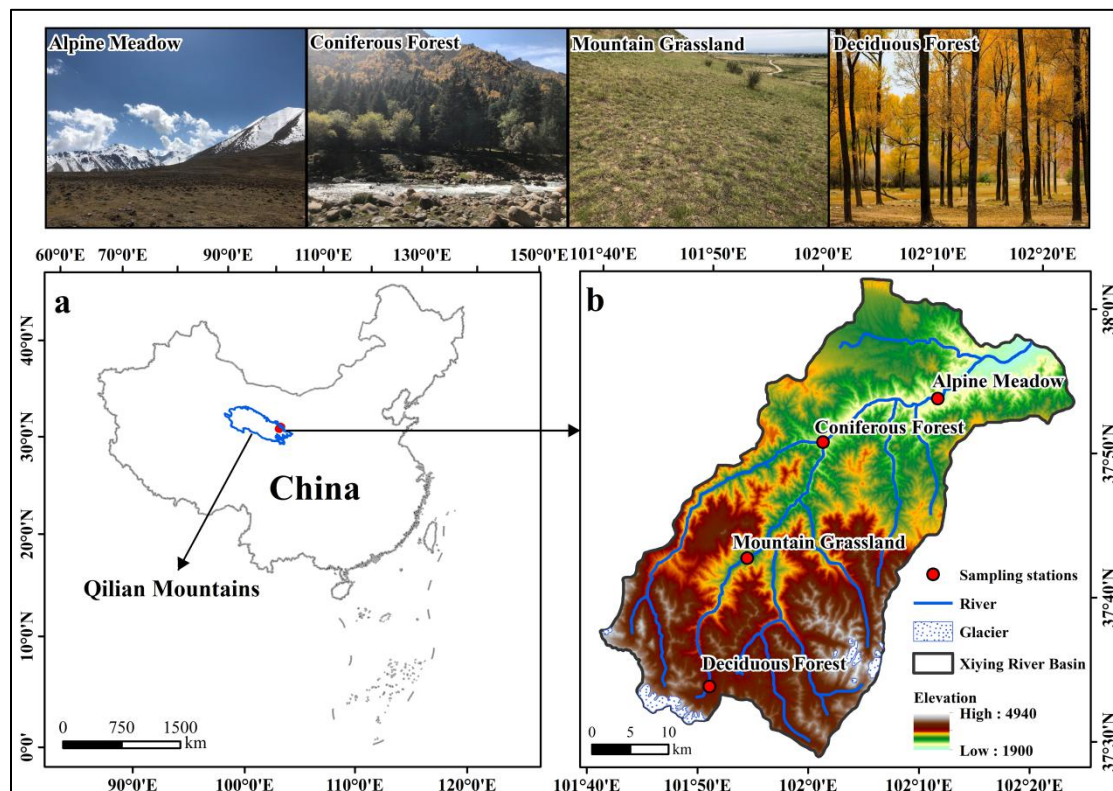
In alpine mountains, climate warming has accelerated the melting of glaciers and frozen soil, and the dynamic interaction between water bodies stored in different media has become the main influencing factor of the water cycle (Penna et al., 2018). Interactions between precipitation and the soil-plant-atmosphere system determine the distribution of water in various storage reservoirs and the subsequent release of water vapor to the atmosphere. These interactions include mainly interception, throughfall, canopy drip, snow accumulation and ablation, infiltration, surface and subsurface runoff, soil moisture, and the partitioning of evapotranspiration between canopy evaporation, transpiration, and soil evaporation. As the main links of the hydrological cycle, these processes have a profound impact on regional water balance and flux distribution.

88 In the past, studies on the evaporation, infiltration and storage of soil water mostly  
89 focused on vegetation types in the same climatic region or different climatic regions.  
90 Understanding the climatic and hydrological conditions of different vertical  
91 vegetation zones and clarifying the regulating role of vegetation in the water cycle can  
92 help better adapt to climate change's influences on the hydrological cycle in source  
93 areas. In this study, we monitored the stable isotope composition of precipitation and  
94 soil water and the spatio-temporal dynamics of soil water storage in four vegetation  
95 zones (alpine meadow, coniferous forest, mountain grassland, and deciduous forest) at  
96 different temperatures and humidity in the Xiying River basin. To explore the  
97 differences in soil water evaporation, infiltration, and storage processes in these four  
98 different climates, vegetation types, and terrain types, the following research  
99 objectives were proposed: (1) to explore the evolution of isotope evaporation signals  
100 and the "memory effects" of precipitation input, mixing and rewetting; (2) to  
101 understand the soil water storage capacity and influencing factors of four vegetation  
102 areas in mountainous areas. It is hoped that this study can further improve the  
103 understanding of the water cycle process and provide a scientific theoretical reference  
104 for water resource utilization and ecological restoration in fragile environments. More  
105 importantly, it can provide paradigms for research at different spatial scales (latitude  
106 zone, longitude zone, watershed, etc.) based on the knowledge of soil moisture  
107 evaporation, infiltration, and water storage in typical vertical vegetation zones.

## 108 **2. Study area**

109 The Xiying River originates from Lenglongling and Kawazhang in the eastern  
110 Qilian Mountains ( $101^{\circ}40'47''\sim102^{\circ}23'5''E$ ,  $37^{\circ}28'22''\sim38^{\circ}1'42''N$ ) (Fig. 1). As  
111 the largest tributary of the Shiyang River, it is formed by the Shuiguan River,  
112 Ningchang River, Xiangshui River, and Tatu River converging from southwest to  
113 northeast and ultimately flowing into the Xiying Reservoir. The average annual runoff  
114 of the Xiying River is 388 million  $m^3$ , which is mainly replenished by mountain  
115 precipitation and melting water of ice and snow. The runoff is mainly concentrated in  
116 summer. The basin elevation is between 2000 m and 5000 m, corresponding to a

117 temperate semiarid climate with strong solar radiation, a long sunshine time, and a  
 118 large temperature difference between day and night. The average annual temperature  
 119 of the basin is 6°C, the annual average evaporation is 1133 mm, the annual average  
 120 precipitation is 400 mm, and the precipitation from June to September accounts for  
 121 69% of the annual precipitation. Precipitation increases with elevation, while  
 122 temperature decreases with elevation in this area (Table 1) (Ma et al., 2018). The  
 123 zonal differentiation of vegetation in the basin is dominated by deciduous forest,  
 124 mountain grassland, cold temperate coniferous forest, and alpine meadow. The soils  
 125 mainly include lime, chestnut, alpine shrub meadow, and desert soil (Fig. 1).



126  
 127 **Fig. 1** Study area and location of sampling points (a. The location of the Xiying  
 128 River Basin in China; b. The terrain and sampling points of the Xiying River Basin)

### 129 **3. Data and methods**

#### 130 **3.1 Sample collection**

131 In this study, soil water and precipitation samples were collected from four  
 132 vegetation zones in the Xiying River basin from April to October in 2017 (plant  
 133 growing season). In 2017, the precipitation in the alpine meadow, coniferous forest,  
 134 mountain grassland and deciduous forest were 595.1 mm, 431.9 mm, 363.5 mm and

135 262.5 mm, respectively. The average daily temperatures in the alpine meadow,  
136 coniferous forest, mountain grassland and deciduous forest were -0.19°C, 3.34°C,  
137 6.6°C and 7.9°C, respectively (Table 1).

138 Collection of soil samples: Soil samples were collected once a month at depths  
139 of 0-10, 10-20, 20-30, 30-40, 40-50, 50-60, 60-70, 70-80, 80-90, and 90-100 cm from  
140 the soil layers in the four vegetation zones. Three duplicate samples were collected for  
141 each soil layer. We placed the collected soil sample into a 50 mL glass bottle, sealed  
142 the bottle mouth with Parafilm and marked the sampling date. We froze the sample for  
143 storage until experimental analysis. Each sample was collected separately in an  
144 aluminum box.

145 Collection of precipitation samples: The precipitation samples were collected by  
146 a plastic funnel bottle device. After each precipitation event, the collected  
147 precipitation samples were immediately transferred to an 80 mL high-density  
148 polyethylene bottle, and the bottle mouth of the samples was sealed with Parafilm;  
149 these samples were also frozen and stored until experimental analysis.

150 Meteorological data: During the sampling period, the local meteorological data  
151 were obtained and recorded by automatic weather stations (Watchdog 2000 series  
152 weather stations) set up near the sample plot.

153 **Table 1** Basic data of each Vegetation zone from April to October 2017 (*Long*-Longitude,  
154 *Lat*-Latitude, *Alt*-Altitude, *T*-Air Temperature (daily mean temperature), *P*-Precipitation (total  
155 precipitation during the observation period), *h*-Relative Humidity (daily mean relative humidity))

Vegetation zone	Geographical parameters			Meteorological parameters			Number of samples	
	<i>Long</i> (°E)	<i>Lat</i> (°N)	<i>Alt</i> (m)	<i>T</i> (°C)	<i>P</i> (mm)	<i>h</i> (%)	Precipitation	Soil
Alpine Meadow	101°51'16"	37°33'28"	3637	-0.19	595.1	69.2	72	47
Coniferous Forest	101°53'23"	37°41'50"	2721	3.34	431.9	66.6	42	41
Mountain Grassland	102°00'25"	37°50'23"	2390	6.6	363.5	60.4	37	54
Deciduous Forest	102°10'56"	37°53'27"	2097	7.9	262.5	59.8	40	53

156 **3.2 Sample determination**

157 The analysis of  $\delta^2\text{H}$  and  $\delta^{18}\text{O}$  values of all the above water samples was  
158 completed using a liquid water isotope analyzer (DLT-100, Los Gatos Research, USA)  
159 in the stable isotope laboratory of Northwest Normal University. Before analyzing the  
160 isotope values of soil water, the soil water was extracted from the collected soil  
161 samples by a low-temperature vacuum condensation system (LI-2100, LICA United  
162 Technology Limited, China). Both the water and isotope standard samples were  
163 injected 6 times during the analysis. To avoid the “memory effect” of isotope analysis,  
164 we discarded the first two injection values and used the average value of the last four  
165 injections as the final result (Penna et al., 2012; Qu et al., 2020). The analysis results  
166 were relative to VSMOW (Vienna Standard Mean Ocean Water):

$$\delta = \left( \frac{R_{\text{sample}}}{R_{\text{standard}}} - 1 \right) \times 1000\% \quad (1)$$

167 where  $R_{\text{sample}}$  is the ratio of  $^{18}\text{O}/^{16}\text{O}$  or  $^2\text{H}/^1\text{H}$  in the sample and  $R_{\text{standard}}$  is the ratio of  
168  $^{18}\text{O}/^{16}\text{O}$  or  $^2\text{H}/^1\text{H}$  in the VSMOW. The test error of the  $\delta^2\text{H}$  value does not exceed  
169  $\pm 0.6\%$ , and the test error of the  $\delta^{18}\text{O}$  value does not exceed  $\pm 0.2\%$ .

### 170 3.3 Analysis method

#### 171 3.3.1 Lc-excess

172 The linear relationship between  $\delta^2\text{H}$  and  $\delta^{18}\text{O}$  in precipitation and soil water is  
173 defined as the LMWL (local meteoric water line) and SWL (soil waterline),  
174 respectively, which are of great significance for studying the evaporative fractionation  
175 of stable isotopes during the water cycle. We further calculated the line-conditioned  
176 excess for each soil water and precipitation sample. The lc-excess in different water  
177 bodies can characterize the evaporation index of different water bodies relative to the  
178 local precipitation (Landwehr and Coplen, 2006).

$$\text{lc-excess} = \delta^2\text{H} - a \times \delta^{18}\text{O} - b \quad (2)$$

179 where  $a$  and  $b$  are the slope and intercept of the LMWL, respectively, and  $\delta^2\text{H}$  and  
180  $\delta^{18}\text{O}$  are the isotopic values of hydrogen and oxygen in the sample. The physical  
181 meaning of lc-excess is expressed as the degree of deviation of the isotope value in  
182 the sample from the LMWL, indicating the nonequilibrium dynamic fractionation

183 process caused by evaporation. Generally, the change in lc-excess in local  
184 precipitation is mainly affected by different water vapor sources, and the annual  
185 average is 0. Since the stable isotopes in soil water are enriched by evaporation, the  
186 average lc-excess is usually negative (Landwehr et al., 2014; Sprenger et al., 2017).

### 187 **3.3.2 Potential evapotranspiration**

188 The potential evapotranspiration was calculated based on the Penman-Monteath  
189 equation (Allen, 1998):

$$190 \text{ PET} = \frac{0.408\Delta(R_n - G) + \gamma \frac{900}{T + 273} u^2 (e_s - e_a)}{\Delta + \gamma(1 + 0.34u^2)} \quad (3)$$

190 where PET is the daily potential evapotranspiration (mm day<sup>-1</sup>),  $R_n$  is the net radiation  
191 (MJ m<sup>2</sup> day<sup>-1</sup>),  $G$  is the soil heat flux density (MJ m<sup>2</sup> day<sup>-1</sup>),  $\gamma$  is the psychrometric  
192 constant (kPa°C<sup>-1</sup>),  $u_2$  is the wind speed at 2 m height (m s<sup>-1</sup>),  $T$  is the mean daily air  
193 temperature at 2 m height (°C),  $\Delta$  is the slope of the vapor pressure curve (kPa°C<sup>-1</sup>),  $e_a$   
194 is the actual vapor pressure (kPa) and  $e_s$  is the saturated vapor pressure (kPa). These  
195 data come from nearby weather stations.

### 196 **3.3.3 Soil water storage**

197 Soil water storage is the thickness of the water layer formed by all the water in a  
198 certain soil layer (Milly, 1994) and is expressed by the following formula:

$$199 S = R \times W \times H \times 10 \quad (4)$$

200 where  $S$  is the soil water storage in a certain thickness layer (mm),  $R$  is the soil bulk  
201 density (g cm<sup>-3</sup>), and  $H$  is the soil thickness (cm).  $W$  is the gravimetric water content,  
202 which is expressed by the following formula:

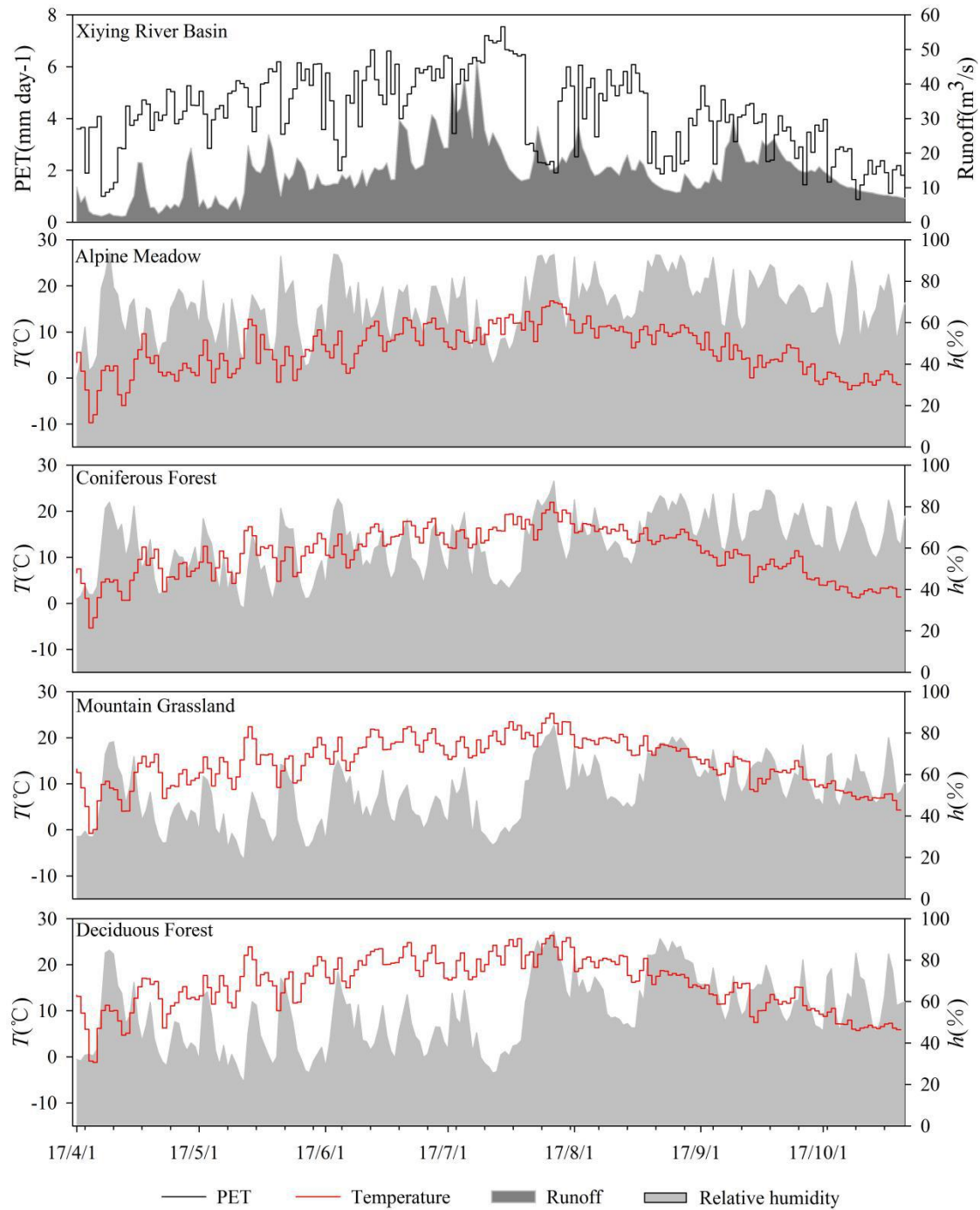
$$203 W = \frac{M_1 - M_2}{M_2} \times 100\% \quad (5)$$

204 in the formula,  $M_1$  is the gravimetric value of wet soil (g), and  $M_2$  is the gravimetric  
205 value of dry soil (g).

## 206 **4. Results and analysis**

### 207 **4.1 Hydrological climate**

206 PET and runoff are important indicators that reflect the dry-wet conditions of  
207 river basins. During the study period (April-October 2017), in the Xiying River Basin,  
208 the potential evapotranspiration was 872.8 mm, the daily evapotranspiration ranged  
209 from 7.5 mm (July 14) to 0.9 mm (October 9), showing a fluctuating trend around  
210 July, and the PET value in April-July was higher than that in August-October. The  
211 input of summer precipitation and ice/snow meltwater increased runoff, resulting in a  
212 trend similar to PET. During the observation period, the total runoff was  $3.1 \times 10^9$  m,  
213 accounting for 89% of the annual runoff. The variation range of the daily runoff was  
214 286848 m<sup>3</sup> (April 17) to 6125760 m<sup>3</sup> (July 13). The basin before July was drier than  
215 that after July (Fig. 2).



216

217 **Fig. 2** Climatic and hydrological conditions of Xiying River basin and its vegetation  
218 zones

219 To explore the differences in the natural environment in different vegetation  
220 zones, air temperature, atmospheric humidity, and precipitation were used to indicate  
221 each research site's temperature and moisture conditions. The hilltop is a typical  
222 alpine meadow zone, with a daily average temperature of 6.1°C, ranging from -9.7°C

223 (April 5) to 16.8°C (July 27). The daily average humidity was 68.2%, with little  
224 difference in different periods. During the observation period, there were 72  
225 precipitation events in the alpine meadow zone, and the total precipitation was 534.3  
226 mm, which was relatively evenly distributed each month. In the coniferous forest zone,  
227 the daily average temperature during the study period was 10.9°C, ranging from  
228 -5.4°C (April 5) to 22.0°C (July 27). The daily average humidity was 62.5%, and the  
229 precipitation was 400.6 mm, mainly concentrated from early August to late September.  
230 Close to the foothills is the mountain grassland zone, with a daily average temperature  
231 of 14.9°C, ranging from -0.7°C (April 5) to 25.3°C (July 27). The average daily  
232 humidity was 51.1%, and the precipitation of the vegetation zone during the  
233 observation period was 327.2 mm, mainly from late July to mid-August. During the  
234 observation period, the daily average temperature in the deciduous forest zone was  
235 15.8°C, ranging from -1.2°C (April 6) to 26.3°C (July 27). The daily average  
236 humidity was 54.7%, and the total precipitation was 250.6 mm, which was  
237 concentrated in the month from late July to late August. The temperatures of the  
238 studied regions were ordered as follows: AM (alpine meadow) < CF (coniferous  
239 forest) < MG (mountain grassland) < DF (deciduous forest). The humidities of the  
240 studied regions were ordered as follows: AM > CF > MG > DF (Fig. 2).

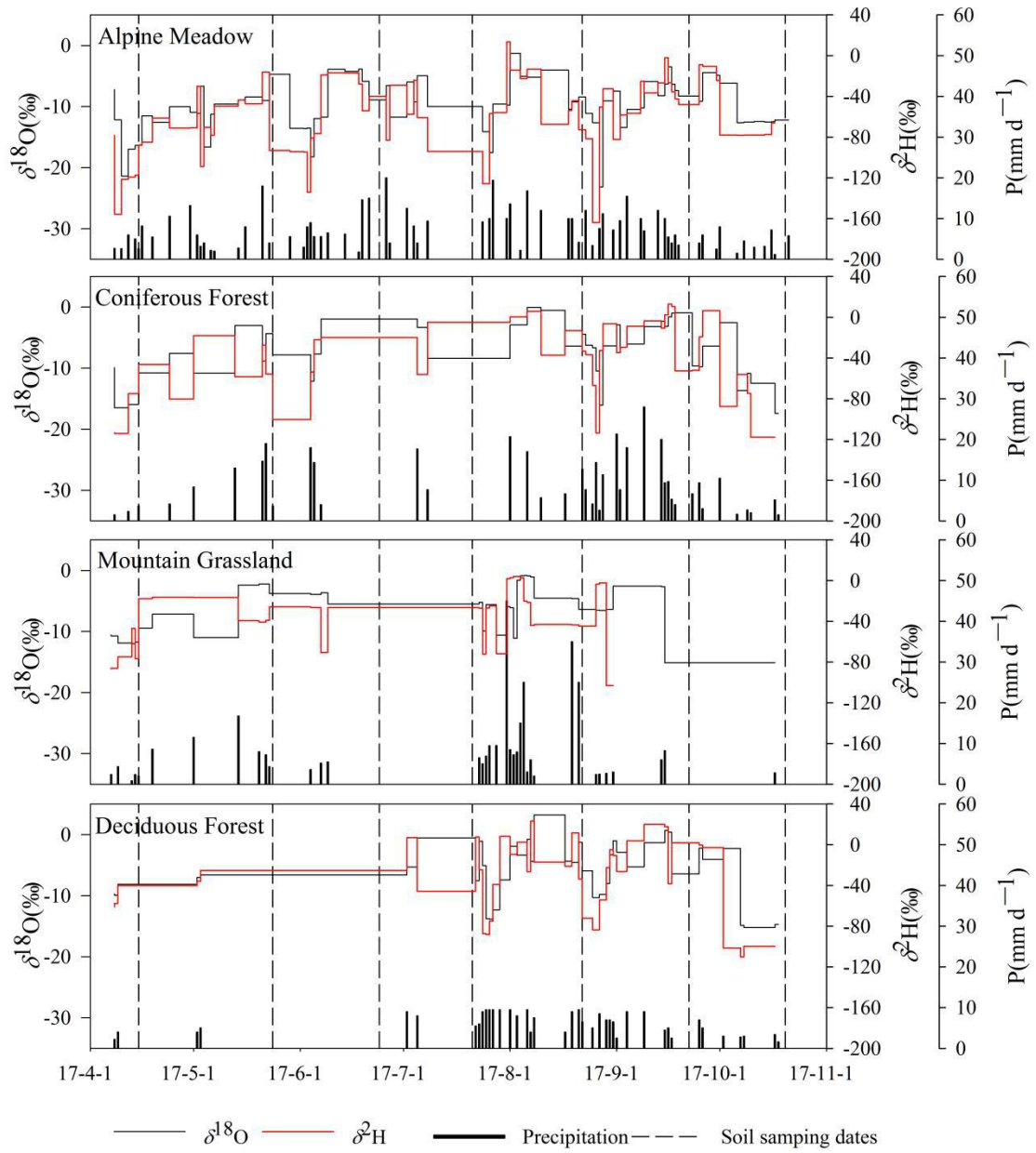
#### 241 **4.2 Temporal variation in water stable isotopes in different vegetation zones**

242 Influenced by different water sources and complex weather conditions in the  
243 precipitation process, the isotopic compositions of precipitation in the four vegetation  
244 zones were different during the study period. The mean values of  $\delta^2\text{H}$  and  $\delta^{18}\text{O}$  in the  
245 alpine meadow zone (number of samples: 72) were  $-73.1\text{\textperthousand}\pm36.3\text{\textperthousand}$  (-163.9~13.7‰)  
246 and  $-10.0\text{\textperthousand}\pm4.3\text{\textperthousand}$  (-23.1~-1.3‰), respectively. The average  $\delta^2\text{H}$  and  $\delta^{18}\text{O}$  values of  
247 the coniferous forest zone (number of samples: 42) were  $-42.0\text{\textperthousand}\pm37.2\text{\textperthousand}$   
248 (-117.8~13.0‰) and  $-7.1\text{\textperthousand}\pm4.7\text{\textperthousand}$  (-17.4~-0.1‰), respectively. The average  $\delta^2\text{H}$  and  
249  $\delta^{18}\text{O}$  values of the mountain grassland zone (number of samples: 37) were  
250  $-37.4\text{\textperthousand}\pm30.5\text{\textperthousand}$  (-103.1~4.2‰) and  $-5.9\text{\textperthousand}\pm3.9\text{\textperthousand}$  (-15.1~-0.9‰), respectively. The  
251 average  $\delta^2\text{H}$  and  $\delta^{18}\text{O}$  values of the deciduous forest zone (number of samples: 40)  
252 were  $-31.8\text{\textperthousand}\pm42.8\text{\textperthousand}$  (-110.2~23.2‰) and  $-5.8\text{\textperthousand}\pm5.5\text{\textperthousand}$  (-15.2~3.2‰), respectively

253 (Table 2). The maximum isotopic values of the four vegetation zones appeared on  
 254 August 4 (AM: 13.7‰,  $\delta^2\text{H}$ ; -1.3‰,  $\delta^{18}\text{O}$ ), August 10 (CF: 13.0‰,  $\delta^2\text{H}$ ; -0.1‰,  
 255  $\delta^{18}\text{O}$ ), August 7 (MG: 4.2‰,  $\delta^2\text{H}$ ; -0.9‰,  $\delta^{18}\text{O}$ ) and August 13 (DF: 23.2‰,  $\delta^2\text{H}$ ;  
 256 3.2‰,  $\delta^{18}\text{O}$ ). The highest temperature in each vegetation zone appeared on July 27.  
 257 The high temperature caused the precipitation to undergo strong below-cloud  
 258 evaporation during the fall, leading to the enrichment of isotopes. In addition, the  
 259 atmospheric precipitation isotopes of the four vegetation zones had similar temporal  
 260 variations: from April to August, the fluctuations in  $\delta^2\text{H}$  and  $\delta^{18}\text{O}$  increased, reached  
 261 the maximum in mid-August, and then gradually decreased (Fig. 3).

262 **Table 2** General characteristics of precipitation  $\delta^2\text{H}$  and  $\delta^{18}\text{O}$  in different vegetation areas  
 263 from April to October 2017

Vegetation zone	$\delta^2\text{H}/\text{‰}$				$\delta^{18}\text{O}/\text{‰}$			
	Max	Min	mean	SD	Max	Min	mean	SD
AM	13.7	-163.9	-73.1	36.3	-1.3	-23.1	-10.0	4.3
CF	13.0	-117.8	-42.0	37.2	-0.1	-17.4	-7.1	4.7
MG	4.2	-103.1	-37.4	30.5	-0.9	-15.1	-5.9	3.9
DF	23.2	-110.2	-31.8	42.8	3.2	-15.2	-5.8	5.5



264

265 **Fig. 3** Time series of rainfall and isotope characteristics in different vegetation  
 266 zones in Xiying River Basin, with dotted lines indicating the date of soil water  
 267 sampling

268 The monthly variation in soil water isotopes records the signal of precipitation  
 269 input and evaporation. The low-temperature environment and abundant precipitation  
 270 events in the alpine meadow make the monthly average  $\delta^2\text{H}$  and  $\delta^{18}\text{O}$  of soil water  
 271 more depleted than other vegetation zones (-69.4~ -51.6 ‰,  $\delta^2\text{H}$ ; -7.5~ -10.3 ‰,  $\delta^{18}\text{O}$ ).  
 272 Despite this, the SWlc-excess of most samples at this station was still negative, and  
 273 there were different degrees of evaporation in the process of precipitation penetrating

274 the soil and mixing with original pore water, among which evaporation fractionation  
275 was stronger in July (-11.9‰ lc-excess) and October (-14.5‰ lc-excess). The soil  
276 water isotopes of the coniferous forest gradually changed seasonally. From April to  
277 July, precipitation was scarce, the temperature rose, and the isotopes of soil water  
278 were gradually enriched on the surface (-52.7~-29.5‰,  $\delta^2\text{H}$ ; -7.0~-2.1‰,  $\delta^2\text{H}$ ),  
279 reaching the peak value of the observation period in July (-29.5‰,  $\delta^2\text{H}$ ; -2.1‰,  $\delta^{18}\text{O}$ ),  
280 and continuous rainfall input from late July to mid-August resulted in soil water  
281 isotope depletion (-57.0‰,  $\delta^2\text{H}$ ; -8.1‰,  $\delta^{18}\text{O}$ ). SWlc-excess was an obvious  
282 fractionation signal opposite to the trend of isotope change, reaching the lowest value  
283 (-26.3‰) in the sampling period in July, and the change in air temperature and  
284 precipitation controlled the evaporation intensity. From April to July, the isotopic  
285 value of surface soil water in the mountain grassland was higher ( $\delta^{18}\text{O}$  was greater  
286 than zero), and SWlc-excess was lower than -30‰. During this period, the  
287 evaporation and fractionation of shallow soil water were intense. Similar to in the  
288 coniferous forest, in the mountain grassland, the input of heavy precipitation from late  
289 July to mid-August led to the depletion of soil water isotopes. There was only  
290 sporadic rainfall in the deciduous forest from April to July, and the soil water isotopes  
291 were gradually enriched on the surface (-46.1~-18.2‰,  $\delta^2\text{H}$ ; -4.7~0.2‰,  $\delta^2\text{H}$ ),  
292 reached a peak in June when there was no rainfall event (-18.2‰,  $\delta^2\text{H}$ ; 0.2‰,  $\delta^{18}\text{O}$ ),  
293 and then became depleted (-53.2‰,  $\delta^2\text{H}$ ; -5.2‰,  $\delta^{18}\text{O}$ ). In addition, due to the  
294 influence of the Xiying Reservoir and vegetation coverage, the isotopic enrichment  
295 degree of soil water in this vegetation zone was lower than that in the mountain  
296 grassland. As the most intuitive form of water change, the gravimetric water content  
297 was always at a low value in July (AM: 21.0%; CF: 14.8%; MG: 11.9%; DF: 14.9%),  
298 when the evaporation was the strongest, and it was most obvious in shallow soil  
299 (Table 3) (Fig. 4).

300

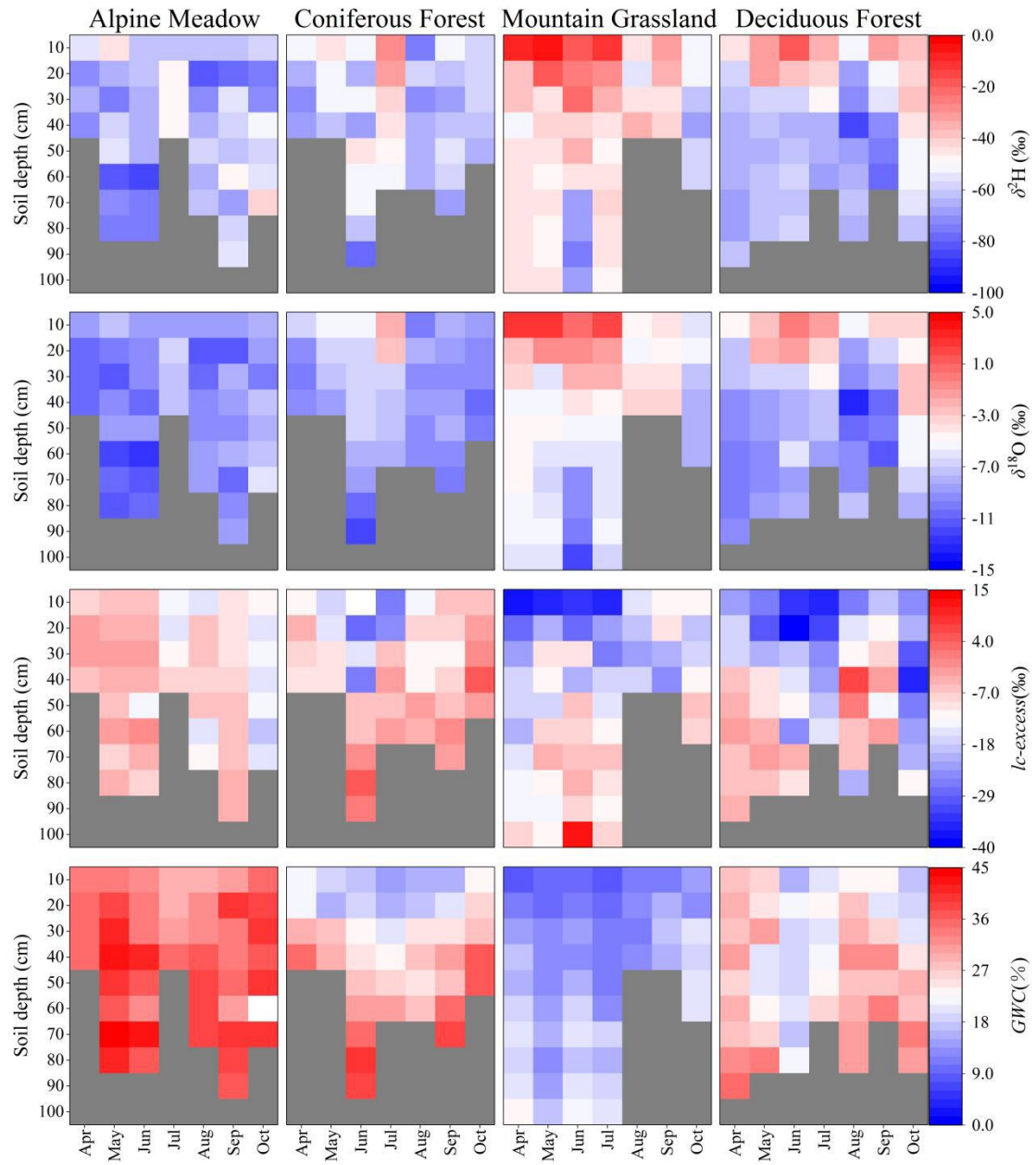
301

302

303

**Table 3** General characteristics of soil water  $\delta^2\text{H}$ ,  $\delta^{18}\text{O}$ , lc-excess and GWC in different  
304 vegetation areas from April to October 2017

Month	Vegetation zone	$\delta^2\text{H}/\text{‰}$			$\delta^{18}\text{O}/\text{‰}$			lc-excess/‰			GWC/%		
		Max	Min	Mean	Max	Min	Mean	Max	Min	Mean	Max	Min	Mean
4	AM	-55.2	-70.7	-65.6	-8.5	-10.8	-10.1	-2.7	-7.1	-4.7	25.9	23.0	24.7
	CF	-52.7	-72.2	-63.9	-7.0	-9.9	-8.9	-4.0	-12.0	-8.4	27.6	14.9	20.0
	MG	-7.32	-50.6	-41.0	2.8	-5.8	-3.9	-8.8	-36.8	-19.4	21.7	6.5	14.7
5	DF	-46.1	-69.4	-62.1	-4.7	-9.9	-8.5	-2.5	-23.2	-9.7	27.7	19.4	21.8
	AM	-46.1	-76.5	-66.4	-7.4	-12.2	-10.1	-2.6	-7.7	-4.9	32.6	23.2	28.9
	CF	-45.8	-61.9	-53.5	-5.3	-8.4	-7.0	-9.3	-17.7	-13.0	22.6	9.0	16.1
6	MG	-6.7	-47.3	-39.2	2.9	-6.5	-4.3	-4.5	-36.2	-14.4	15.7	7.6	11.2
	DF	-30.8	-63.5	-53.8	-1.9	-9.4	-6.9	-3.2	-30.1	-13.6	26.0	11.7	17.7
	AM	-62.5	-83.9	-69.4	-8.9	-12.6	-10.3	-1.5	-8.4	-5.8	33.3	21.9	26.0
7	CF	-45.8	-78.4	-58.7	-5.1	-12.0	-7.8	5.5	-26.6	-8.5	32.1	10.0	21.3
	MG	-19.7	-74.9	-46.9	0.8	-11.8	-5.8	13.0	-33.7	-11.0	19.3	7.5	14.2
	DF	-18.2	-64.9	-51.7	0.2	-9.0	-5.9	-4.6	-38.2	-19.4	13.5	8.4	11.1
8	AM	-47.3	-60.1	-51.6	-6.9	-8.4	-7.5	-8.8	-14.8	-11.9	25.4	19.0	21.0
	CF	-29.5	-51.4	-41.6	-2.1	-7.9	-5.6	-2.6	-26.3	-11.2	24.3	7.2	14.8
	MG	-10.6	-48.4	-39.2	2.3	-6.4	-4.1	-5.8	-35.8	-16.1	18.7	6.3	11.9
9	DF	-35.1	-69.0	-54.1	-1.7	-8.7	-5.5	-14.8	-35.3	-24.5	18.2	11.8	14.4
	AM	-58.5	-80.3	-66.6	-8.4	-11.6	-9.6	-6.1	-15.4	-9.7	28.1	19.5	25.1
	CF	-57.0	-75.5	-66.4	-8.1	-9.8	-9.2	-2.5	-13.1	-8.3	21.4	8.7	16.3
10	MG	-34.2	-53.8	-44.0	-3.2	-5.5	-4.4	-14.7	-22.6	-18.7	11.3	9.5	10.4
	DF	-53.2	-84.3	-67.6	-5.2	-13.5	-9.2	6.8	-26.1	-9.6	23.6	14.7	20.6
	AM	-48.0	-79.2	-61.0	-7.8	-11.1	-9.2	-4.3	-10.4	-7.2	29.9	20.3	25.3
9	CF	-52.5	-67.7	-60.7	-7.8	-10.1	-8.8	-0.1	-11.3	-6.0	31.3	9.3	20.5
	MG	-32.3	-45.3	-38.8	-3.5	-4.4	-4.0	-9.1	-23.8	-16.5	15.3	9.1	13.0
	DF	-30.5	-77.0	-59.8	-3.1	-11.4	-8.2	-1.8	-19.3	-9.3	25.8	14.7	19.1
10	AM	-42.4	-73.5	-58.9	-6.1	-9.8	-7.9	-12.2	-18.2	-14.5	36.2	25.4	29.5
	CF	-59.1	-66.3	-61.7	-8.8	-10.5	-9.5	5.1	-5.3	-1.5	30.0	16.8	23.1
	MG	-50.3	-66.7	-58.3	-5.6	-8.3	-7.1	-5.5	-18.4	-11.9	18.3	11.4	15.8
	DF	-38.0	-61.8	-48.3	-2.7	-8.2	-4.9	-11.9	-34.8	-23.9	25.5	8.9	17.2

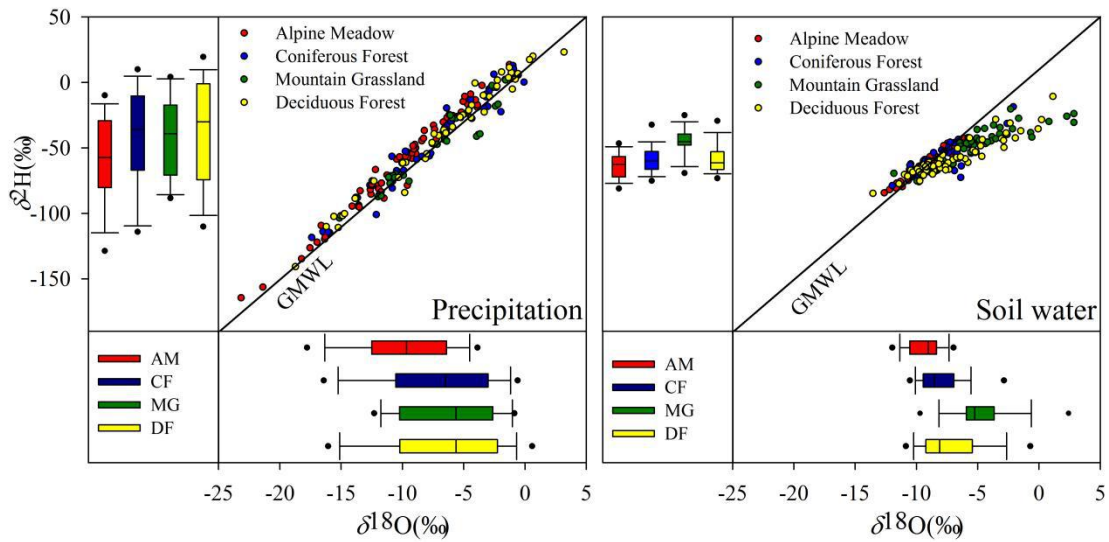


305  
 306 **Fig. 4** Heat map of the soil depth profile of  $\delta^2\text{H}$ ,  $\delta^{18}\text{O}$ , *lc-excess* and GWC in  
 307 different vegetation zones, and the layer lacking measurement is indicated by the  
 308 grey color

309 **4.3 Spatial variation in water stable isotopes in different vegetation zones**

310 Isotope data of precipitation and soil water obtained from different vegetation  
 311 zones are shown in dual-isotope space in Fig. 5. At the alpine meadow observation  
 312 station, the slope (8.4) and intercept (23) of the LMWL were higher than those of the  
 313 GMWL. The slope of the LMWL in the other three vegetation zones was lower than  
 314 that of the GMWL and gradually decreased with decreasing altitude. With the

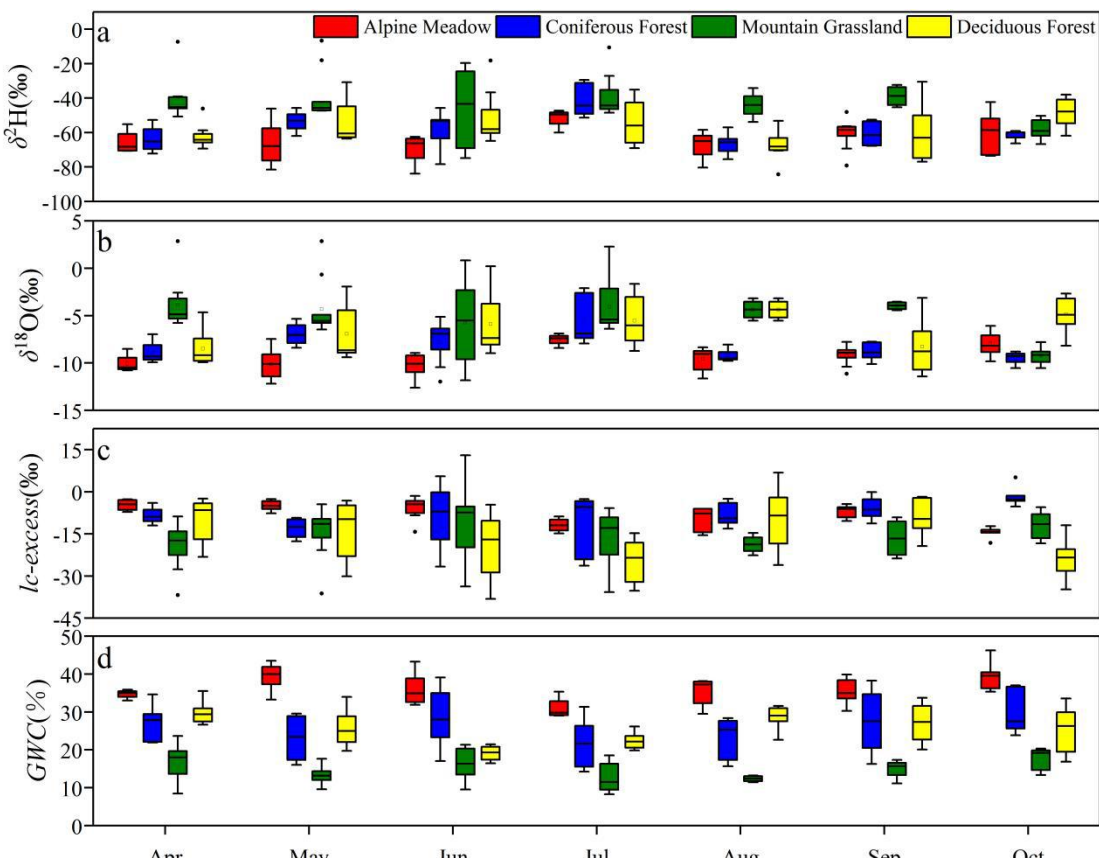
315 decrease in altitude, the slope of the SWL in all vegetation zones except for the  
 316 deciduous forest SWL decreased (AM: 6.4; CF: 4.7; MG: 3.4; DF: 4.1), indicating  
 317 that the evaporation of soil moisture increased. On the one hand, the vegetation  
 318 coverage of the deciduous forest site was higher. On the other hand, the Xiying  
 319 Reservoir enhanced the regional air humidity and decreased the local water vapor  
 320 circulation driving force.



321  
 322 **Fig. 5** Dual-isotope space of precipitation (left) and soil water (right) isotope data of  
 323 four vegetation zones. In the box plots, the box represents the 25%-75% percentile,  
 324 the line in the box represents the median (50th percentile), the required line  
 325 indicates 90th and 10th percentile, and the point indicates the 95th and 5th  
 326 percentile.

327 During the study period, compared with that in other vegetation belts, the surface  
 328 isotopic value of the soil water in the mountain grassland was relatively enriched  
 329 (-24.3‰, δ<sup>2</sup>H; -0.8‰, δ<sup>18</sup>O), the lc-excess was smaller and deeper into the middle  
 330 and lower soil layers (-25.8‰), and the gravimetric water content was relatively low  
 331 (8.4%). Due to the difference in vegetation types and the influence of reservoirs, this  
 332 change did not have an obvious elevation effect. Although the elevation was low, the  
 333 soil water of the deciduous forest had more depleted isotopic characteristics and  
 334 higher soil moisture than those of the mountain grassland in most samples. Soil  
 335 profiles obtained from different vegetation zones can reflect the evaporation signals of

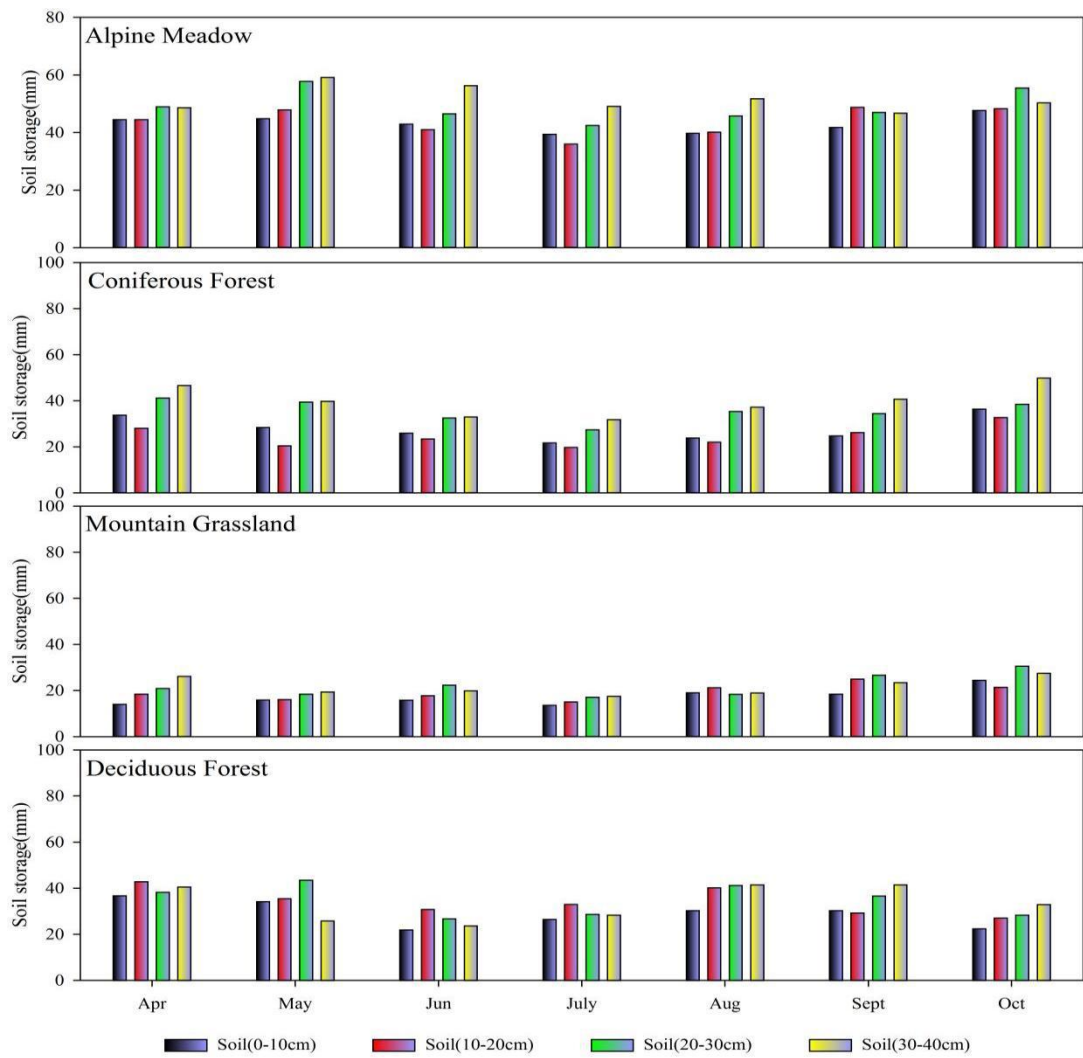
water. The low-temperature natural environment made alpine meadow soil less affected by evaporation ( $lc\text{-excess} > -20\text{\textperthousand}$ ), and the gravimetric water content was high (gravimetric water content  $> 20\%$ ) during the whole study period. The surface soil water of the coniferous forest was easily affected by climate and had a higher isotopic composition ( $-29.5\text{\textperthousand}$ ,  $\delta^2\text{H}$ ;  $-2.1\text{\textperthousand}$ ,  $\delta^{18}\text{O}$ ) and lower  $lc\text{-excess}$  ( $-26.3\text{\textperthousand}$ ). Due to evaporation, soil water isotopes in the mountain grassland and deciduous forest areas were enriched in the surface soil layer. In particular, in the mountain grassland, the average values of  $\delta^2\text{H}$  and  $\delta^{18}\text{O}$  in the 0-10 cm soil layer were as high as  $-24.4\text{\textperthousand}$  and  $-1.2\text{\textperthousand}$ , respectively, and  $SWlc\text{-excess}$  was lower than  $-25\text{\textperthousand}$ , even close to  $-40\text{\textperthousand}$  in some samples. In this case, the evaporation signals can easily penetrate the deep soil, making the gravimetric water content values at all the sampling sites lower than 20% (Fig. 4; Fig. 6).



348  
349 **Fig. 6** The variation of  $\delta^2\text{H}$ ,  $\delta^{18}\text{O}$ ,  $lc\text{-excess}$  and  $GWC$  in different vegetation zones  
350 in each sampling

351 **4.4 Variations in the water storage capacity of the 0-40 cm soil layer in different  
352 vegetation areas**

353 This study used soil water to calculate the water storage of the 0-40 cm soil layer  
354 in the four vegetation zones during the observation period (Fig 7). The water storage  
355 capacity of the alpine meadow gradually decreased from April to July (209.7~167.2  
356 mm), and the water storage capacity increased after July (167.2~201.8 mm). The  
357 monthly average water storage capacity was the lowest at 0-10 cm (43.0 mm) and the  
358 highest at 30-40 cm (51.7 mm). The water storage capacity of the coniferous forest  
359 gradually decreased from April to July (150.1~101.2 mm), and the water storage  
360 capacity increased after July (101.2~160.0 mm). The monthly average water storage  
361 capacity was the lowest at 0-10 cm (28.0 mm) and the highest at 30-40 cm (40.0 mm).  
362 The water storage capacity of the mountain grassland gradually decreased from April  
363 to July (80.3~64.0 mm), and the water storage capacity increased after July  
364 (64.0~104.6 mm). The monthly average water storage capacity was the lowest at 0-10  
365 cm (17.5 mm) and the highest at 20-30 cm (22.0 mm). The water storage capacity of  
366 the deciduous forest gradually decreased from April to June (159.3~104.0 mm), the  
367 water storage capacity increased from June to August (104.0~154.0 mm), and there  
368 was a decrease from August to October (154.0~111.8 mm). The monthly average  
369 water storage capacity was the lowest at 0-10 cm (29.1 mm) and the highest at 20-30  
370 cm (35.0 mm). In general, the soil water storage capacity of the 0-10 cm soil layer  
371 was less than that of the other soil layers. The order of the water storage capacity of  
372 the 0-40 cm soil layer in the four vegetation zones is alpine meadow (46.9 mm) >  
373 deciduous forest (33.0 mm) > coniferous forest (32.1 mm) > mountain grassland (20.3  
374 mm).



375

376 **Fig. 7** Monthly variation of soil water storage in 0-40cm soil layer of different  
 377 vegetation zones

378 **5. Discussion**

379 **5.1 Evaporation of soil moisture in different vegetation zones**

380 In the arid river source area, the replenishment of soil moisture mainly comes  
 381 from precipitation. The slope of the regional atmospheric precipitation line can reflect  
 382 the strength of local evaporation. Due to a low atmospheric temperature, low cloud  
 383 base height, and low air-saturated water vapor loss, the alpine meadow zone was  
 384 weakly affected by secondary evaporation during precipitation. There, the slope of the  
 385 LMWL (8.4) was even higher than that of the GMWL (Hughes and Crawford, 2012).  
 386 As the altitude decreased, the secondary evaporation under clouds strengthened, and

387 the slope of the LMWL of each vegetation zone decreased (Pang et al., 2011). The  
388 slope of SWL can indicate the strength of soil moisture evaporation in each vegetation  
389 zone, the evaporation intensity results of the four vegetation zones followed the order  
390 of mountain grassland ( $SWL_{slop}$ : 3.4) > deciduous forest ( $SWL_{slop}$ : 4.1) > coniferous  
391 forest ( $SWL_{slop}$ : 4.7) > alpine meadow ( $SWL_{slop}$ : 6.4) (Fig 5). The dynamic changes in  
392 lc-excess of soil profiles in different vegetation areas reflect the process of soil water  
393 evaporation caused by drought during the study period. The monthly average value of  
394  $SWL_{lc}$ -excess in the alpine meadow zone was less than 0, and the minimum value was  
395 -11.9‰ (July). Although the vegetation belt was subject to different degrees of  
396 evaporation each month, it was less affected by drought, and it was difficult for  
397 evaporation to penetrate into the middle and lower soil layers. The  $SWL_{lc}$ -excess of the  
398 coniferous forest belt was greater than that of the alpine meadow from April to June.  
399 The evaporation was the strongest in July (-11.2‰ lc-excess). Similar to in the alpine  
400 meadow, in the coniferous forest belt, evaporation mainly occurred in the topsoil. The  
401 vegetation coverage of the mountain grassland zone was low, and the arid  
402 environment made the isotopes of the surface soil produce strong evaporation signals  
403 (lc-excess was close to -40‰). In most samples, the  $SWL_{lc}$ -excess of the 60-80 cm soil  
404 layer was negative. The evaporation signal shifted to the lower layer of the soil  
405 (Barnes and Allison, 1988; Zimmermann et al., 1966). Similar evaporation signals  
406 have been found in the Mediterranean and arid climate regions (McCutcheon et al.,  
407 2017; Sprenger et al., 2016). Evaporation signals exist in only the surface soil in  
408 humid areas, and there is no difference between lc-excess and 0 in the soil layer below  
409 20 cm (Sprenger et al., 2017). The monthly surface soil evaporation of deciduous  
410 forest was less than that of mountain grassland from April to June, and it was greater  
411 than that of mountain grassland after July, mainly due to the influence of the  
412 vegetation and reservoirs. There were commonalities in the soil moisture changes in  
413 different vegetation zones characterized by more enriched isotopes, stronger  
414 evaporation signals, and lower moisture content in the shallow soil. With increasing  
415 soil depth, the isotope gradually became depleted, and the evaporation signal was  
416 gradually weakened until it disappeared. The evolution of the investigated isotopes,

417  $\delta^{18}\text{O}$ -excess, and gravimetric water content in the unsaturated soil showed differences  
418 among different vegetation zones. From a high altitude to a low altitude, the isotopic  
419 value of the surface gradually increased, and the evaporation signal increased (Fig 4;  
420 Fig 6).

421 **5.2 Memory effects of precipitation input, mixing and rewetting**

422 The changes in soil water isotopes and soil moisture can evaluate the input,  
423 mixing, and rewetting precipitation process in different vegetation areas. The main  
424 methods of precipitation input are plug flow and preferential flow. Plug flow is the  
425 complete mixing of water through the soil matrix with shallow free water. Under the  
426 action of plug flow, precipitation infiltrates along the hydraulic gradient, pushing the  
427 original soil water downward. Preferential flow means that precipitation uses soil  
428 macropores to quickly penetrate shallow soil to form deep leakage (Tang and Feng,  
429 2001). After precipitation, the variability of isotope signals at a certain soil depth can  
430 identify the seepage method of water (Peralta-Tapia et al., 2015). During the study  
431 period, the soils of the alpine meadow and coniferous forest areas were seasonally  
432 frozen and thawed year-round, and the difference in the soil isotope profile was small.  
433 The soil moisture profile showed a trend of water increasing from top to bottom,  
434 indicating the influence of the previous precipitation. The soil was humid, so the  
435 replenishment of soil water by precipitation had the characteristics of top-down piston  
436 replenishment. Preferential infiltration showed high variability in isotopic signals  
437 (Brodersen et al., 2000), and the rainwater in mountain grassland and deciduous forest  
438 flowed into the deep soil rapidly through the soil matrix via exposed soil fissures and  
439 roots. This resulted in the sudden depletion of soil isotopes at a depth of 60-100 cm.  
440 This may be due to the more recent depleted precipitation that quickly reached this  
441 depth and the preferential infiltration into the soil. Water movement and mixing in the  
442 unsaturated zone can be observed in the spatiotemporal variation in isotopes within 1  
443 m of the soil profile, and the alpine meadow and coniferous forest zones underwent  
444 considerable rainfall. After a short period of weak evaporation, the soil was rewetted  
445 by the next rainfall. In the alpine meadow, the soil moisture remained above 20% each  
446 month. The mountain grassland and deciduous forest zones had only sporadic

447 precipitation from mid-May to late July, and the soil moisture evaporated rapidly.  
448 With the decrease in air temperature and the occurrence of continuous precipitation  
449 after July, the soil was rewetted after two months of drought, and both vegetation  
450 zones showed the replacement and mixing of soil water isotopes and precipitation.  
451 The results showed that the soil water storage capacity of the alpine grassland was  
452 seriously insufficient, reflecting the incomplete rewetting of the soil by precipitation  
453 at the end of the study. In addition, low soil water storage capacity will enrich the  
454 remaining soil water isotopes (Barnes and Allison, 1988; Zimmermann et al., 1966).  
455 We observed the memory effect of soil rewetting caused by precipitation input and the  
456 mixing of different vegetation areas during the entire study period. The changes in  
457 soil moisture in each vegetation area reflect different climatic and hydrological  
458 characteristics (Fig. 4; Fig. 6).

459 **5.3 Influencing factors of soil water storage capacity in arid headwater areas**

460 As the temperature decreased rapidly with increasing height, precipitation and  
461 humidity increased to a certain extent, and the vegetation showed a strip-like  
462 alternation approximately parallel to the contour line, forming zonal vegetation with  
463 obvious differentiation (Yin et al., 2020). The dry-wet conditions of different  
464 vegetation zones restricted the soil water storage capacity in the basin. In the process  
465 of low-altitude vegetation zone replacement, the precipitation decreased, the  
466 temperature rose, the groundwater level dropped, and the soil water storage capacity  
467 was weak (Coussement et al., 2018; Kleine et al., 2020). The soil water storage  
468 capacity of the alpine meadow zone with low-temperature and rainy weather was  
469 higher than that of other vegetation zones (results of the 0-40 cm soil layers from  
470 April to October: AM: 187.8 mm; CF: 128.4 mm; MG: 81.2 mm; DF: 132.1 mm).  
471 During the study period, the soil water storage capacity (0-40 cm) exceeded 165 mm  
472 each month. With the decrease in altitude, the monthly difference in dry-wet  
473 conditions in each vegetation zone gradually became obvious. With the increase in  
474 temperature in summer, the environment became dry, and the soil water storage  
475 capacity weakened (Sprenger et al., 2017). The soil water storage capacity of the  
476 coniferous forest zone began to decrease in April, and the water storage capacity of

477 the 0-40 cm layer reached the minimum value (101.2 mm) in July. The variation in  
478 temperature and precipitation was the main reason for the monthly difference  
479 (Dubber and Werner, 2019). Although there was a certain water storage capacity in  
480 the coniferous forest with some transpiration loss, the soil water storage capacity in  
481 this vegetation zone was not strong. The water storage capacity of mountain grassland  
482 soil was lower than that of other vegetation zones. The continuous dry and warm  
483 weather in spring and summer led to the water storage capacity of 0-40 cm soil being  
484 lower than that of 100 mm every month. In particular, drought stress leads to  
485 insufficient soil moisture, making it difficult to maintain plant demand, resulting in  
486 sparse vegetation and large-scale exposed surface soil, which further accelerates  
487 surface water loss. The continuous precipitation from the end of July prevented  
488 further drought development, and the water input gradually restored the soil water  
489 storage capacity (Kleine et al., 2020). The deciduous forest had hydrothermal  
490 conditions similar to those of the mountain grassland, but the soil porosity of the  
491 forest zone was obviously larger than that of the barren land, and its permeability was  
492 higher than that of the barren land. Precipitation infiltrated the ground through roots  
493 and turned into groundwater. The forest acted as a reservoir due to its strong water  
494 storage and soil conservation capacity (Sprenger et al., 2019). The water storage  
495 capacity of the 0-40 cm soil layer in the deciduous forest was higher than 100 mm at  
496 each sampling time. In addition, the water content of the 0-40 cm soil layer in each  
497 vegetation zone increased with the deepening of the soil layer, and the water storage  
498 capacity of the surface soil was weak. The difference in soil properties also led to  
499 more water storage in the middle and lower soil layers with higher clay contents  
500 (Milly, 1994) (Fig. 7). Climate warming and the spatiotemporal imbalance of water  
501 resources have disturbed the ecological-water balance of different vegetation zones in  
502 inland river source areas (Liu et al., 2015). Plant growth mainly depends on the water  
503 stored in shallow soil layers (Amin et al., 2020). Drought reduces soil water storage  
504 and inhibits plant growth (Li et al., 2020). To effectively improve and manage water  
505 resources in arid water source areas, exploring the heterogeneity of hydrological

506 processes among different vegetation zones is necessary. This will provide a reference  
507 for the formulation of ecological policies.

508 **6. Conclusion**

509 This work provides further insights into the movement and mixing of soil water in  
510 different vegetation zones in arid source regions. During the study period, the  
511 dynamic changes in  $lc$ -excess in the soil profiles of different vegetation zones  
512 reflected the evaporation signals caused by drought. Soil water evaporation in spring  
513 and summer and insufficient precipitation during the drought period were the main  
514 driving forces of isotopic enrichment in the surface soil. The soil water evaporation  
515 intensity results of the four vegetation zones followed the order of mountain grassland  
516 ( $SWL_{slop}$ : 3.4) > deciduous forest ( $SWL_{slop}$ : 4.1) > coniferous forest ( $SWL_{slop}$ : 4.7) >  
517 alpine meadow ( $SWL_{slop}$ : 6.4). In the mountain grassland and deciduous forest zones,  
518 drought caused the evaporation signal to penetrate deep into the middle and lower soil  
519 layers. The  $SWlc$ -excess below 70 cm of the ground surface remained negative. Soil  
520 water isotopes and gravimetric water content record the process of soil rewetting  
521 caused by precipitation input and mixing. The alpine meadow and coniferous forest  
522 zones were enriched in precipitation. After a short period of weak evaporation, the  
523 soil was rewetted by the next precipitation event. There was only sporadic  
524 precipitation in the mountain grassland and deciduous forest belt from mid-May to  
525 late July. After July, the temperature dropped, and continuous precipitation wet the  
526 soil again after two months of drought. The mountain grassland and deciduous forest  
527 zones had only sporadic precipitation from mid-May to late July. With the decrease in  
528 air temperature and continuous precipitation after July, the soil was rewetted after two  
529 months of drought. Moisture and temperature conditions were the key factors that  
530 restricted the soil water storage capacity in the different vegetation zones. The water  
531 storage capacity of the 0-40 cm soil layer results followed the order of alpine meadow  
532 (46.9 mm) > deciduous forest (33.0 mm) > coniferous forest (32.1 mm) > mountain  
533 grassland (20.3 mm). The water storage capacity of the surface soil in each vegetation  
534 zone was weak, and more water was stored in the middle and lower soil layers with

535 higher clay contents. The research results can be applied to arid and semi-arid alpine  
536 regions and have reference significance for latitude and longitude differentiation. This  
537 study mainly emphasized the Spatio-temporal heterogeneity of soil water evaporation,  
538 infiltration, and water storage in different vegetation zones. These results are of great  
539 value for understanding regional hydrological processes and ecological restoration  
540 services in environmentally fragile areas. Furthermore, we hope this study can be used  
541 as a basic statement because we continue to use stable water isotopes as a data source  
542 to understand hydrological processes from the perspective of process mechanisms.

## 543 **References**

544 Allen, R. G.: Crop evapotranspiration :guidelines for computing crop water requirements, FAO  
545 irrigation and drainage paper, edited, Food and Agriculture Organization of the United Nations,  
546 Rome, 300 pp., 1998.

547 Amin, A., Zuecco, G., Geris, J., Schwendenmann, L., McDonnell, J. J., Borga, M., and Penna, D.:  
548 Depth distribution of soil water sourced by plants at the global scale: A new direct inference  
549 approach, *Ecohydrology*, 13, e2177, <https://doi.org/10.1002/eco.2177>, 2020.

550 Barnes, C. J., and Allison, G. B.: Tracing of water movement in the unsaturated zone using stable  
551 isotopes of hydrogen and oxygen, *J. Hydrol.*, 100, 143-176,  
552 [https://doi.org/10.1016/0022-1694\(88\)90184-9](https://doi.org/10.1016/0022-1694(88)90184-9), 1988.

553 Brodersen, C., Pohl, S., Lindenlaub, M., Leibundgut, C., and Wilpert, K. V.: Influence of  
554 vegetation structure on isotope content of throughfall and soil water, *Hydrol. Process.*, 14,  
555 1439-1448,  
556 [https://doi.org/10.1002/1099-1085\(20000615\)14:8<1439::AID-HYP985>3.0.CO;2-3](https://doi.org/10.1002/1099-1085(20000615)14:8<1439::AID-HYP985>3.0.CO;2-3), 2000.

557 Brooks, R. J., Barnard, H. R., Coulombe, R., and McDonnell, J. J.: Ecohydrologic separation of  
558 water between trees and streams in a Mediterranean climate, *Nat. Geosci.*, 3, 100-104,  
559 <https://doi.org/10.1038/ngeo722>, 2010.

560 Coussette, T., Maloteau, S., Pardon, P., Artru, S., Ridley, S., Javaux, M., and Garré, S.: A  
561 tree-bordered field as a surrogate for agroforestry in temperate regions: Where does the water  
562 go? *Agr. Water Manage.*, 210, 198-207, <https://doi.org/10.1016/j.agwat.2018.06.033>, 2018.

563 Dansgaard, W.: Stable isotopes in precipitation, *Tellus*, 16, 436-468,  
564 <https://doi.org/10.3402/tellusa.v16i4.8993>, 1964.

565 Dubbert, M., and Werner, C.: Water fluxes mediated by vegetation: emerging isotopic insights at  
566 the soil and atmosphere interfaces, *New Phytologist*, 221, 1754-1763,  
567 <https://doi.org/10.1111/nph.15547>, 2019.

568 Duvert, C., Stewart, M. K., Cendón, D. I., and Raiber, M.: Time series of tritium, stable isotopes  
569 and chloride reveal short-term variations in groundwater contribution to a stream, *Hydrol. Earth  
570 Syst. Sci.*, 20, 257-277, <https://doi.org/10.5194/hess-20-257-2016>, 2016.

571 Ferretti, D. F., Pendall, E., Morgan, J. A., Nelson, J. A., LeCain, D., and Mosier, A. R.:  
572 Partitioning evapotranspiration fluxes from a Colorado grassland using stable isotopes:  
573 Seasonal variations and ecosystem implications of elevated atmospheric CO<sub>2</sub>, *Plant Soil*, 254,

574 291-303, <https://doi.org/10.1023/A:1025511618571>, 2003.

575 Gibson, J. J., Holmes, T., Stadnyk, T. A., Birks, S. J., Eby, P., and Pietroniro, A.: Isotopic  
576 constraints on water balance and evapotranspiration partitioning in gauged watersheds across  
577 Canada, *Journal of Hydrology: Regional Studies*, 37, 100878,  
578 <https://doi.org/10.1016/j.ejrh.2021.100878>, 2021.

579 Grant, G. E., and Dietrich, W. E.: The frontier beneath our feet, *Water Resour. Res.*, 53,  
580 2605-2609, <https://doi.org/10.1002/2017WR020835>, 2017.

581 Hughes, C. E., and Crawford, J.: A new precipitation weighted method for determining the  
582 meteoric water line for hydrological applications demonstrated using Australian and global  
583 GNIP data, *J. Hydrol.*, 464-465, 344-351, <https://doi.org/10.1016/j.jhydrol.2012.07.029>, 2012.

584 Kleine, L., Tetzlaff, D., Smith, A., Wang, H., and Soulsby, C.: Using water stable isotopes to  
585 understand evaporation, moisture stress, and re-wetting in catchment forest and grassland soils  
586 of the summer drought of 2018, *Hydrol. Earth Syst. Sci.*, 24, 3737-3752,  
587 <https://doi.org/10.5194/hess-24-3737-2020>, 2020.

588 Koeniger, P., Gaj, M., Beyer, M., and Himmelsbach, T.: Review on soil water isotope-based  
589 groundwater recharge estimations, *Hydrol. Process.*, 30, 2817-2834,  
590 <https://doi.org/10.1002/hyp.10775>, 2016.

591 Landwehr, J. M., and Coplen, T. B.: Line-conditioned excess: a new method for characterizing  
592 stable hydrogen and oxygen isotope ratios in hydrologic systems, International conference on  
593 isotopes in environmental studies, 2006, 132-135, 2006.

594 Landwehr, J. M., Coplen, T. B., and Stewart, D. W.: Spatial, seasonal, and source variability in the  
595 stable oxygen and hydrogen isotopic composition of tap waters throughout the USA, *Hydrol.  
596 Process.*, 28, 5382-5422, <https://doi.org/10.1002/hyp.10004>, 2014.

597 Li, X., Piao, S., Wang, K., Wang, X., Wang, T., Ciais, P., Chen, A., Lian, X., Peng, S., and  
598 Peñuelas, J.: Temporal trade-off between gymnosperm resistance and resilience increases forest  
599 sensitivity to extreme drought, *Nature Ecology & Evolution*, 4, 1075-1083,  
600 <https://doi.org/10.1038/s41559-020-1217-3>, 2020.

601 Liu, Y., Liu, F., Xu, Z., Zhang, J., Wang, L., and An, S.: Variations of soil water isotopes and  
602 effective contribution times of precipitation and throughfall to alpine soil water, in Wolong  
603 Nature Reserve, China, *Catena*, 126, 201-208, <https://doi.org/10.1016/j.catena.2014.11.008>,  
604 2015.

605 Ma, X., Jia, W., Zhu, G., Ding, D., Pan, H., Xu, X., Guo, H., Zhang, Y., and Yuan, R.: Stable  
606 isotope composition of precipitation at different elevations in the monsoon marginal zone,  
607 *Quatern. Int.*, 493, 86-95, <https://doi.org/10.1016/j.quaint.2018.06.038>, 2018.

608 McCutcheon, R. J., McNamara, J. P., Kohn, M. J., and Evans, S. L.: An evaluation of the  
609 ecohydrological separation hypothesis in a semiarid catchment, *Hydrol. Process.*, 31, 783-799,  
610 <https://doi.org/10.1002/hyp.11052>, 2017.

611 Milly, P. C. D.: Climate, soil water storage, and the average annual water balance, *Water Resour.  
612 Res.*, 30, 2143-2156, <https://doi.org/10.1029/94WR00586>, 1994.

613 Pang, Z., Kong, Y., Froehlich, K., Huang, T., Yuan, L., Li, Z., and Wang, F.: Processes affecting  
614 isotopes in precipitation of an arid region, *Tellus B: Chemical and Physical Meteorology*, 63,  
615 352-359, <https://doi.org/10.1111/j.1600-0889.2011.00532.x>, 2011.

616 Penna, D., Hopp, L., Scandellari, F., Allen, S. T., Benettin, P., Beyer, M., Geris, J., Klaus, J.,  
617 Marshall, J. D., Schwendenmann, L., Volkmann, T. H. M., von Freyberg, J., Amin, A.,

618 Ceperley, N., Engel, M., Frentress, J., Giambastiani, Y., McDonnell, J. J., Zuecco, G., Llorens,  
619 P., Siegwolf, R. T. W., Dawson, T. E., and Kirchner, J. W.: Ideas and perspectives: Tracing  
620 terrestrial ecosystem water fluxes using hydrogen and oxygen stable isotopes – challenges and  
621 opportunities from an interdisciplinary perspective, *Biogeosciences*, 15, 6399-6415,  
622 <https://doi.org/10.5194/bg-15-6399-2018>, 2018.

623 Penna, D., Stenni, B., Šanda, M., Wrede, S., Bogaard, T. A., Michelini, M., Fischer, B. M. C.,  
624 Gobbi, A., Mantese, N., Zuecco, G., Borga, M., Bonazza, M., Sobotková, M., Čejková, B., and  
625 Wassenaar, L. I.: Technical Note: Evaluation of between-sample memory effects in the analysis  
626 of  $\delta^{2\text{H}}$  and  $\delta^{18\text{O}}$  of water samples measured by laser spectrometers, *Hydrol. Earth  
627 Syst. Sci.*, 16, 3925-3933, <https://doi.org/10.5194/hess-16-3925-2012>, 2012.

628 Peralta-Tapia, A., Sponseller, R. A., Tetzlaff, D., Soulsby, C., and Laudon, H.: Connecting  
629 precipitation inputs and soil flow pathways to stream water in contrasting boreal catchments,  
630 *Hydrol. Process.*, 29, 3546-3555, <https://doi.org/10.1002/hyp.10300>, 2015.

631 Qu, D., Tian, L., Zhao, H., Yao, P., Xu, B., and Cui, J.: Demonstration of a memory calibration  
632 method in water isotope measurement by laser spectroscopy, *Rapid Commun. Mass Sp.*, 34,  
633 e8689, <https://doi.org/10.1002/rcm.8689>, 2020.

634 Rothfuss, Y., and Javaux, M.: Reviews and syntheses: Isotopic approaches to quantify root water  
635 uptake: a review and comparison of methods, *Biogeosciences*, 14, 2199-2224,  
636 <https://doi.org/10.5194/bg-14-2199-2017>, 2017.

637 Sharma, H., Ehlers, T. A., Glotzbach, C., Schmid, M., and Tielbörger, K.: Effect of rock uplift and  
638 Milankovitch timescale variations in precipitation and vegetation cover on catchment  
639 erosion rates, *Earth Surf. Dynam.*, 9, 1045-1072, <https://doi.org/10.5194/esurf-9-1045-2021>,  
640 2021.

641 Snelgrove, J. R., Buttle, J. M., Kohn, M. J., and Tetzlaff, D.: Co-evolution of xylem water and soil  
642 water stable isotopic composition in a northern mixed forest biome, *Hydrol. Earth Syst. Sci.*, 25,  
643 2169-2186, <https://doi.org/10.5194/hess-25-2169-2021>, 2021.

644 Sprenger, M., Leistert, H., Gimbel, K., and Weiler, M.: Illuminating hydrological processes at the  
645 soil-vegetation-atmosphere interface with water stable isotopes, *Rev. Geophys.*, 54, 674-704,  
646 <https://doi.org/10.1002/2015RG000515>, 2016.

647 Sprenger, M., Llorens, P., Cayuela, C., Gallart, F., and Latron, J.: Mechanisms of consistently  
648 disjunct soil water pools over (pore) space and time, *Hydrol. Earth Syst. Sci.*, 23, 2751-2762,  
649 <https://doi.org/10.5194/hess-23-2751-2019>, 2019.

650 Sprenger, M., Tetzlaff, D., and Soulsby, C.: Soil water stable isotopes reveal evaporation  
651 dynamics at the soil–plant–atmosphere interface of the critical zone, *Hydrol. Earth Syst. Sci.*,  
652 21, 3839-3858, <https://doi.org/10.5194/hess-21-3839-2017>, 2017.

653 Tang, K., and Feng, X.: The effect of soil hydrology on the oxygen and hydrogen isotopic  
654 compositions of plants' source water, *Earth Planet. Sc. Lett.*, 185, 355-367,  
655 [https://doi.org/10.1016/S0012-821X\(00\)00385-X](https://doi.org/10.1016/S0012-821X(00)00385-X), 2001.

656 Tetzlaff, D., Soulsby, C., Buttle, J., Capell, R., Carey, S. K., Laudon, H., McDonnell, J., McGuire,  
657 K., Seibert, J., and Shanley, J.: Catchments on the cusp? Structural and functional change in  
658 northern ecohydrology, *Hydrol. Process.*, 27, 766-774, <https://doi.org/10.1002/hyp.9700>, 2013.

659 Xiao, W., Wei, Z., and Wen, X.: Evapotranspiration partitioning at the ecosystem scale using the  
660 stable isotope method—A review, *Agr. Forest Meteorol.*, 263, 346-361,  
661 <https://doi.org/10.1016/j.agrformet.2018.09.005>, 2018.

662 Yin, L., Dai, E., Zheng, D., Wang, Y., Ma, L., and Tong, M.: What drives the vegetation dynamics  
663 in the Hengduan Mountain region, southwest China: Climate change or human activity? *Ecol.*  
664 *Indic.*, 112, 106013, <https://doi.org/10.1016/j.ecolind.2019.106013>, 2020.

665 Zhu, G., Yong, L., Zhang, Z., Sun, Z., Sang, L., Liu, Y., Wang, L., and Guo, H.: Infiltration  
666 process of irrigation water in oasis farmland and its enlightenment to optimization of irrigation  
667 mode: Based on stable isotope data, *Agr. Water Manage.*, 258, 107173,  
668 <https://doi.org/10.1016/j.agwat.2021.107173>, 2021a.

669 Zhu, G., Yong, L., Zhang, Z., Sun, Z., Wan, Q., Xu, Y., Ma, H., Sang, L., Liu, Y., Wang, L., Zhao,  
670 K., and Guo, H.: Effects of plastic mulch on soil water migration in arid oasis farmland:  
671 Evidence of stable isotopes, *Catena*, 207, 105580, <https://doi.org/10.1016/j.catena.2021.105580>,  
672 2021b.

673 Zimmermann, U., Münnich, K. O., Roether, W., Kreutz, W., Schubach, K., and Siegel, O.: Tracers  
674 Determine Movement of Soil Moisture and Evapotranspiration, *Science*, 152, 346-347,  
675 <https://doi.org/10.1126/science.152.3720.346>, 1966.

## 676 **Acknowledgments**

677 This research was financially supported by the National Natural Science  
678 Foundation of China (41661005, 41867030, 41971036). The authors much thank the  
679 colleagues in the Northwest Normal University for their help in fieldwork, laboratory  
680 analysis, data processing.

## 681 **Author Contribution statement**

682 Guofeng Zhu and Leilei Yong conceived the idea of the study; Yuanxiao Xu and  
683 Qiaozhuo Wan analyzed the data; Zhigang Sun and Leilei Yong were responsible for  
684 field sampling; Zhuanxia Zhang participated in the experiment; Lei Wang participated  
685 in the drawing; Leilei Yong wrote the paper; Liyuan Sang, Xi Zhao and Yuwei Liu  
686 checked and edited language. All authors discussed the results and revised the  
687 manuscript.

## 688 **Additional Information**

689 Competing Interests: The authors declare no competing interests.